Biofabrication

International Society for Biofabrication

PURPOSE-LED PUBLISHING™

Pneumatic conveying inkjet bioprinting for the processing of living cells

To cite this article before publication: Justyna Bożek *et al* 2025 *Biofabrication* in press https://doi.org/10.1088/1758-5090/ada8e2

IOP Publishing Journal Title
Journal **XX** (XXXX) XXXXXX https://doi.org/XXXX/XXXX

Pneumatic conveying inkjet bioprinting for the processing of living cells

Justyna Bożek[1], Olga Kurchakova[2], Johanna Michel[2], Isabel Groß[2], Lena Gerhards[1], Yangzhen Zhang[3], Izabella Brand[1,4]*, Anja U. Bräuer[2,4]*

[1] Department of Chemistry, Carl von Ossietzky Universität Oldenburg, Oldenburg, Germany
[2] Research Group Anatomy, School for Medicine and Health Science, Carl von Ossietzky Universität Oldenburg, Oldenburg, Germany
[3] College of Mechanical and Electronic Engineering, China University of Petroleum (East China), Qingdao, 266580, China
[4] Research Center for Neurosensory Science, Carl von Ossietzky Universität Oldenburg, Oldenburg, Germany

E-mail: Izabella Brand: izabella.brand@uni-oldenburg.de; Anja Bräuer: anja.brauer@uni-oldenburg.de

Received xxxxxx
Accepted for publication xxxxxx
Published xxxxxx

Abstract

Inkjet printing techniques are often used for bioprinting purposes because of their excellent printing characteristics, such as high cell viability and low apoptotic rate, contactless *modus operandi*, commercial availability, and low cost. However, they face some disadvantages, such as the use of bioinks of low viscosity, cell damage due to shear stress caused by drop ejection and jetting velocity, as well as a narrow range of available bioinks that still challenge the inkjet printing technology. New technological solutions are required to overcome these obstacles. Pneumatic conveying printing, a new type of inkjet-based printing technique, was applied for the bioprinting of both acellular and cellular fibrin-hydrogel droplets. Drops of a bioink containing 6×10^6 HEK293H cells/ml were supplied from a sterile nozzle connected to a syringe pump and deposited on a gas stream on a fibrinogen-coated glass slide, here referred to as biopaper. Fibrinogen film is the substrate of the polymerization reaction with thrombin and Ca^{2+} present in the bioink.
The pneumatic conveying printing technique operates on a mechanism by which drop ejection and deposition in a stream of gas occurs. The percentage of unprinted and printed dead HEK293H cells was 5 ± 2 % and 7 ± 4 %, respectively. Thus, compared to normal handling, pneumatic conveying printing causes only little damage to the cells. The velocity of the drop approaching the biopaper surface is below 0.2 m/s and does not cause any damage to the cells. The cell viability of printed cells was 93%, being an excellent value for inkjet printing technology. The HEK293H cells exhibited approximately a 24 h lag time of proliferation that was preceded by intense migration and aggregation. Control experiments proved that the cell migration and lag time were associated with the chemical nature of the fibrin hydrogel and not with cell stress.

Keywords: inkjet bioprinting, pneumatic conveying printing, fibrin, HEK cells

1. Introduction

Bioprinting is a group of additive manufacturing technologies aiming at the designed assembly of biologically relevant materials in 2D and 3D structures that accomplish one or more biological functions. Four bioprinting technologies are commonly used in this novel research field: extrusion, inkjet (droplet-based), laser-assisted, and stereolithographic printing.[1-5] Despite extensive work and substantial progress in bioprinting technology, each of the existing techniques suffers from limitations that include resolution, maintenance of shape, availability of bioinks and their stability, as well as the preservation of biological functions. Below, inkjet printing techniques are described with the focus on their applicability for bioprinting purposes.

Inkjet printing is a droplet-based printing technology in which small-volume ink drops are produced on demand and deposited in the desired location: the printing occurs at a high speed.[2; 6-12] Piezo inkjet and thermal-bubble inkjet are the two main printing technologies. The piezo inkjet uses a quick transformation of the micro piezo ceramic to generate a high-pressure pulse for drop ejection; the thermal bubble inkjet uses a micro heater to vaporize the ink to form a bubble, which pushes the ink out to form drops. In inkjet printing technology, uniform droplets are ejected from a nozzle onto a paper surface with high precision. In the 1970s, thermal inkjet printing was invented by Ichiro Endo at Cannon [13] and Jon Vaught at Hewlett-Packard [14]. In 1980, Robert Howard produced a printing system that used piezo elements to eject a drop of ink.[15] Over the last decades, inkjet printing has become the most commonly used printing technology. Commercial availability and the low cost of inkjet printers make them attractive for bioprinting applications. [2; 16; 17]

Inkjet printing is contactless, indicating that the ink has no contact with the substrate (paper), a characteristic that possesses *in situ* and *in vivo* application potential. [2; 12; 18; 19] In all inkjet printing techniques, bioink drops are ejected from a nozzle. To maintain the shape of the printed structure, an ejected drop of liquid (bioink) must undergo rapid solidification.[2; 12; 20] Hydrogels, binders, powders, polymers, and small molecules have been used to achieve this goal.[2; 21; 22] Among them, hydrogels are the most commonly used in bioprinting technology.[7; 21-24]. These are crosslinked hydrophilic polymer networks that swell in water, holding up to 99.9% of their dry weight of water. The important advantage of hydrogels is their ability to mimic the extracellular matrix (ECM). Regarding their physical, mechanical, and biological properties, hydrogels provide a similar structure to ECM and allow cell communication in three dimensions. Physical and chemical cross-linking types are used to produce hydrogels. For example, alginate hydrogel, obtained after physical cross-linking of L-guluronate residues in the polysaccharide with Ca^{2+} ions, belongs to the most commonly used hydrogels in inkjet printing.[12; 20; 25] However, alginate hydrogel often lacks biocompatibility and is unable to interact with mammalian cells, thus hindering their adhesion, communication, and proliferation.[25] To improve biocompatibility, alginate has been mixed with other biopolymers such as collagen, gelatin, or fibrinogen.[26; 27] Fibrin hydrogel is another widely used natural hydrogel material providing structural support to printed cells.[28] Fibrin is formed during reaction of fibrinogen with thrombin.[29-31] The fibrinogen polymerization reaction is initiated by the cleavage by thrombin of fibrinopeptides A and B at the N-terminus of the protein to produce fibrinogen monomer. Ca^{2+} ions bind to fibrinogen affecting the kinetics and size (length and thickness) of fibrin, the polymerization product. Fibrin possesses elastic and stretchable three-dimensional interconnected randomly arranged fibers.[32; 33] Fibrin is a biodegradable polymer indicating that after printing it may be replaced by extracellular matrix secreted by cells. Clearly, bioink formulation and its post-printing characteristics define the next class of challenges that face bioprinting technologies.

The most commonly used piezo- and thermal inkjet techniques are applicable to inks with a viscosity in the range of 3 – 30 mPa s.[2; 19; 34] However, bioinks with a biological cell density of $> 10^7$ cells/ml have a significantly higher viscosity than is suitable for inkjet printing, thus limiting the application of inkjet printing in tissue- and organ engineering. Printing of 3D structures containing at least two different kinds of cells represent another challenge of bioprinting technology.[12; 35] Furthermore, in liquids with low viscosity, cells may sediment and clog the nozzle.[2; 19] The use of bioinks with biological cell loads is a challenge for commercial printers. Therefore, modifications improving inkjet bioprinting performance are very much required.[36-40]

Below, a few recent improvements in bioprinting technology are reported. Park et al. modified piezoelectric inkjet printing, aiming at a patterned print of different kinds of cells, including complex gradient arrangements.[35] Adenocarcinomic human alveolar basal epithelial cells (A549) and HeLa cells were printed from two nozzles. High-

speed imaging of cell jetting and impacting behaviors allowed for the control of the location of printed cells to generate complex cell patterns on the biopaper surface.

To overcome the problem of the use of low-viscosity bioinks, inkjet techniques using two nozzles have been engineered. In inkjet-spray hybrid printing, one nozzle was used to print layers of a hydrogel. Subsequently, a second nozzle spraying a cross-linking agent was used to endow the printed feature with a stable form.[37] Mouse fibroblasts (NIH3T3), human embryonic kidney cells (293A), and human newborn foreskin fibroblasts (Hs68) were printed from bioinks containing sodium alginate, cellulose, or fibrinogen. The printing of the bioink was followed immediately by spray-printing of an ink containing the crosslinking agent. The use of two nozzles allowed for the fast printing of hydrogels with different geometry, and sizes ranging from μm to cm. [37] Christensen used two nozzles to develop an inserting jet-printing technique.[36] A bioink with a neuronal stem-cell load and cross-linking Ca^{2+} ions was ejected from a nozzle at one printing head, while the sol solution (sodium alginate) was ejected from the nozzle at the second printing head. Both heads were mounted such that the two ejected drops collided mid-air. The two drops joined in air and underwent a fast solidification reaction, yielding a hydrogel (alginate). The hydrogel drops were collected in a liquid bath.

Pneumatic conveying printing is an inkjet printing technology that is almost pressure-free during the printing process and is capable of handling viscous bioinks, and thus being particularly attractive for bioprinting applications.[38; 39] In this technique, a bioink drop, extruded from a hydrophobic orifice, is cut and carried to the biopaper surface in a gas stream. We further improved the biocompatibility and performance of this emerging technique, mainly by modifying the printing head. The bioink is extruded into the air from a sterile needle that is oriented in parallel to the printed surface. The liquid drop is cut by a gas stream flowing from a second needle oriented vertically to the bioink-extruding needle. The position of both needles can be manually adjusted. The printing head can easily be sterilized, and the sterile needles are removed after each printing, preventing any contamination of the bioink. A drop of sol (bioink), ejected from the nozzle. Due to the fact that the droplet is delivered with the gas stream, without droplet flight bending observed in other inkjet printing techniques [41], to a surface of a biopaper that is covered by a drop-solidifying agent. The gelation process occurs immediately after interaction of the bioink with the biopaper, facilitating the drop docking and settlement. One of the limitations of pneumatic conveying printing is a need to use sols that undergo a fast gelation reaction. Among natural hydrogels, alginate and fibrin are the biopolymers most often used in inkjet printing techniques.[42-44] An ideal hydrogel used for bioprinting purposes should provide a matrix supporting the structure for freshly printed cells and, over time, undergo biodegradation, creating space for cell-cell communication, proliferation, and then finally be substituted by the extracellular matrix formed by the cells.

To test the pneumatic conveying printing technique, a bioink with 6 million/ml HEK293H cells was formulated and printed on a fibrinogen biopaper yielding fibrin drops. Our results show that the new technique is gentle to the cells, and the shear stress is low. The cell viability of the freshly printed cells was 93%. In the first 24 h, we did not observe cell proliferation; instead the cells migrated intensively and aggregated. Control experiments demonstrated that the cell migration and lag time in proliferation were associated with the chemical nature of the fibrin hydrogel and not with stress experienced by the cells during the printing.

2. Materials and Methods

2.1. Materials

For the preparation of electrolyte solutions, $CaCl_2 \times 2H_2O$ (VWR International BVBA, Belgium) and NaCl, KCl, KH_2PO_4, $Na_2HPO_4 \times 2H_2O$ (≥99.5% Carl Roth GmbH + Co. KG, Germany) were used. Fibrinogen from human plasma (Cat. No. F3879), thrombin from bovine plasma (Cat. No. T4648), and hexamethyldisilazane (HMDS) were purchased from Sigma Aldrich (Germany). Polylysine (PLL, Cat. No. P2636) was purchased from Merck (Germany). Ethyl alcohol (99.8%) used in SEM experiments was purchased from Fisher Scientific (UK). Chloroform, methanol, ethanol, and the 2-propanol used in all other experiments were from Sigma Aldrich (Germany). DMEM (Dulbecco's Modified Eagle Medium) (Cat. No. P04-03550, Lot: 9820122) was obtained from Pan Biotech GmbH, (Germany). Water (resistivity 18.2 MΩ cm) was purified by the water-purification system Elga Purelab Classic (Elga LabWater, Germany). D_2O for IR spectroscopy experiments was purchased from Euroisotop (UK). Trypan Blue Stain (ThermoFischer Scientific, Waltham, USA) and a Neubauer cell-counting chamber (BRAND® GmbH, Wertheim,

Germany) were used for cell-death measurements. DAPI (4′,6-diamidino-2-phenylindole)-containing mounting medium - ROTI Mount FluorCare (Carl Roth GmbH, Karlsruhe, Germany) was used for cell-proliferation measurements.

2.2 Pneumatic conveying printing

2.2.1 Preparation of the substrate for printing: "Biopaper"

Glass microscope slides (VWR International BVBA, Belgium), cut or whole, were rinsed with water and ethanol and then placed in a UV-ozone cleaner (Bioforce Nanoscience Inc., USA) for 10 minutes. To produce fibrinogen film on the glass surface, 500 µl of 10 mg/ml fibrinogen from human plasma in 0.15 M NaCl solution was dropped on the whole slide, which was placed in a Petri dish. In the case of a cut glass slide, a proportionally smaller volume of fibrinogen solution was dropped on the surface. Such prepared samples were left for at least 12 h for self-assembly, during which a milky protein film appeared on the glass surface. Before printing, the slides were washed with distilled water and dried.

2.2.2 Bioink formulation

For cell printing, HEK293H cells (human embryonic kidney cells, Thermo Fisher Scientific, Waltham, MA, USA; catalog ID 11631017) were routinely maintained in DMEM (PAN-Biotech, Germany) supplemented with 10% FCS (PAN-Biotech), 200 mM L-533 glutamine (Thermo Fisher), and 100 U/ml penicillin/streptomycin (PAN-Biotech) at 37 °C and 5 % CO_2. For the bioink formulation, after trypsinization with 0.05 % trypsin-EDTA (Thermo Fisher) at 37 °C for 3 min, HEK293H cells were collected by centrifugation for 5 min at 1500 rpm, corresponding to 478 rcf. The cell pellet was re-dissolved in DMEM, and the number of cells assessed by counting. The bioinks were prepared from stock solutions of 117.8 mM $CaCl_2$ in DMEM supplemented with 0.1 % FBS, L-533 glutamine and penicillin/streptomycin and 13.2 mg/ml thrombin in DMEM supplemented with 0.1 % FBS. Ampules containing 450 µl and 50µl of the $CaCl_2$ and thrombin stock solutions were prepared, frozen, and used to formulate bioinks. To prepare 2 ml of the acellular bioink 450 µl of the 117.8 mM $CaCl_2$ stock solution and 50 µl 13.2 mg/ml thrombin stock solution and 1500 µl of supplemented DMEM. To prepare 2ml of the cellular bioink 40 IOWA Units/ml thrombin and 1500 µl of 6×10^6 cells/ml in supplemented DMEM. DMEM contains 1.8 mM $CaCl_2$, indicating that the bioink contained 41.8 mM Ca^{2+} ions and 0.33 mg/ml (40 IOWA Units/ml) thrombin. The printing occurred in ambient air. After printing, the samples were immediately placed in a Petri dish in a supplemented DMEM in an incubation chamber (37 °C and 5% CO_2). They were first analyzed 1-2 h, then 24 and 96 h after printing.

The surface energy of the bioink without and with 6×10^6 cells/ml of HEK293H cells was measured using the drop weight method. The liquid was introduced into glass capillaries with an inner diameter of 700 µm. In each independent experiment, 10 drops were collected and their mass determined. As the reference, the measurements were carried out on water and ethanol. The surface energy of the bioink (γ) was determined from equation 1 [23],

$$2\pi r\gamma = \frac{m}{n}g \qquad (1)$$

where r is the radius of the capillary, m – mass of the drops of liquid, n number of collected drops (here10), and g - acceleration due to gravity (9.8 m/s^2).

2.2.3 The printing setup

Pneumatic conveying printing is a new technique [38; 45] that we further modified to increase its applicability for bioprinting purposes. The pneumatic conveying printing set-up used here consisted of a commercial Ender 3 type 3D printing machine (Comgrow, China), a computer-controlled syringe pump (GeSIM XP3000, GESIM, Dresden, Germany), a gas source (Ar or CO_2, Dräger, Lübeck, Germany), and a home-made printing head, see Figure 1.

The printing head provided adjustable holders for two sterile hollow needles with an inner diameter of 160 µm and outer diameter of 300 µm (Figure 1), one straight and the other bent at 45° (G30 cannulas, Gonano Dosierungtechnik, Austria). The needles were mounted orthogonal to each other as required in pneumatic conveying printing [38; 45]. A

bioink drop formed at the nozzle of the bend needle is jetted by a gas stream from a vertically positioned straight needle, see Figure 1B. The gas-delivering needle (1) in Figure 1A is oriented vertically with respect to the biopaper surface. Due to the fact that the droplets travel in the stream of gas, they are delivered on the surface of biopaper, directly under the needle, minimizing the droplet flight bending reported for droplets ejected in air. [41] Ar (testing phase, use of acellular bioinks) or CO_2 (printing of cellular and acellular bioinks) gases were used in the printing experiments. Both gases have similar densities, indicating that the gas flow rates were comparable. The gas flow rate in a pipe with the inner diameter of 2 mm, ranged between 0.6 and 1.0 l/min, resulting in a gas velocity of 1.00 ± 0.24 m/s. Due to reduction of the diameter of the pipe inside the needle, the velocity of the gas at the nozzle was 157 m/s (calculation of the gas velocity in the needle is described in SI Section S1, Figure S1). Due to possible small leakage of the gas at the connection between the gas pipe and the needle, the flow velocity was likely smaller than that calculated.

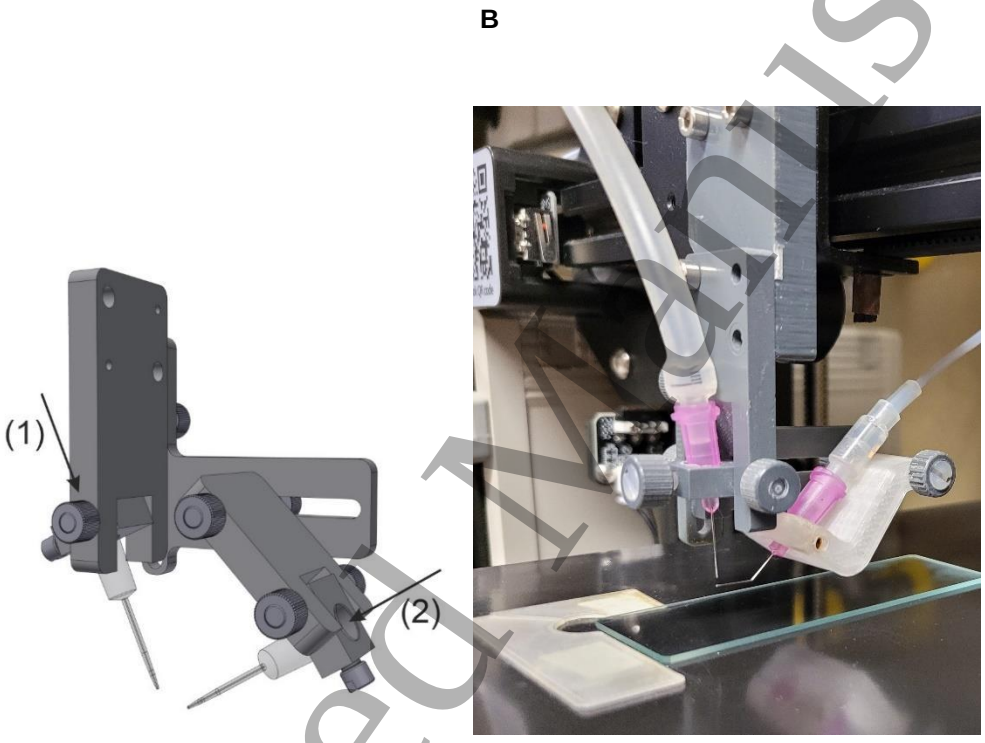

Figure 1. A: Schematic diagram of the printing head mounted on a commercial Ender 3 type 3D printing machine: (1) Gas and (2) Bioink were delivered by separate sterile needles mounted on an adjustable holder. Image created at the Workshop of the University of Oldenburg. Ing. F. Reichig; **B:** a photograph of the printing head and the positioning of the glass slide on the printing table. The distance of the bend needle to the glass surface is 5 mm.

The gas velocity needed to be adjusted to the size of the nozzle delivering the bioink (here R_0 = 80 µm), the surface pressure of the liquid bioink, and the distance between the gas outlet and the ink outlet (approximately 1 mm) affect the quality of printing.[45] In our experiments, the radius of the detached drop was R_d = 345 ± 9 µm . It was larger than size of the needle used for printing due to the fact that the bioink liquid wets the needle. For a drop with the R_d = 345 ± 9 µm the theoretically calculated gas velocity must be larger than 20 m/s.[45] By increasing the gas velocity above 250 m/s (gas flow rate > 1.2 l/s) the drop was moved away in the gas stream and satellite drops were formed. Thus, at high gas flow velocity, the accuracy of the printing was lowered. Decreasing the gas flow velocity to less than 100 m/s (gas flow rate <0.5 l/s) caused an increase in the drop size at the nozzle (R_d) to approximately 1000 µm,

lowering the resolution of the printing. Therefore, it was very important to control the gas flow rate to optimize the resolution and accuracy of the pneumatic conveying printing technique. The resolution of the technique is limited by the size and shape of the needle, surface properties of the ink, and rate of hydrogel formation, as will be discussed in the results and discussion section. [19; 45]

A 45° bent sterile needle (R_0 = 80 µm), delivering the bioink, was placed in the printing head so that its nozzle was oriented parallel to the printed surface, see Figure 1. The bioink was supplied to the needle from the syringe pump. In these experiments, the best results were obtained at the liquid flow rate of 0.42 µl/s, which is in the range of flow rates (0.03 – 1.60 µl/s) used in the electrohydrodynamic jet printing technique [46]. Before printing, all parts of the printer and the syringe pump were sterilized with 70% EtOH and placed in a sterile bench. Ethanol and water were pumped through the syringe pump to keep it sterile and clean. Finally, 0.75 – 1.00 ml of the bioink was introduced into the syringe pump and the needle in the printing head filled with the bioink. A microscope glass substrate covered by a fibrinogen film, the biopaper, was placed on the printing table. The printing pattern was written in a G code, typically used for bioprinting applications.[2; 3; 36] The printing head moved at 11.67 mm/s. The starting position (above the substrate surface) was defined in the program, and the head moved in the plane of the substrate along the X and Y directions. On each glass slide, five lines 25 mm long and separated by 4 mm were printed; 16.7 µl of the bioink was used to print one such pattern. There were 97 ± 5 drops counted during the printing of a glass slide (based on 10 independent experiments), giving an average of 12 ± 1 drops per line. The average volume of a bioink drop dispensed from the syringe was 172 ± 18 nl, indicating that the average radius of the drop detached from the nozzle was R_d = 345 ± 9 µm. The Z direction, normal to the substrate, represents the stand-off distance of the nozzle of the bioink supplying the needle to the substrate surface. The stand-off distance was adjustable but kept constant at ~5 mm. Video analysis of the drop development, cutting, and deposition on the biopaper allowed the estimation of the drop fly velocity approaching the biopaper surface to be ~0.2 m/s, which is low compared to the velocity of the drop jetting in piezoelectric inkjet printing technique (2 – 4 m/s). [11; 18; 47]

2.2.4 Drop shape characterization

The size of the printed drops (top-down perspective) was measured from N = 40 drops by obtaining their horizontal and vertical diameter (Table S1). N corresponds to the number of analyses, whereas n corresponds to the number of independent experiments. To measure the drop height and contact angles, the printed drops were photographed from a side-view perspective within 2 minutes after printing using OCA Dataphysics Instruments GmbH, Germany. Pictures were taken from n = 3 independent printing procedures on different days. For the measurement of the contact angles of the printed drops, N = 57 drops were measured on the first, N = 49 on the second, and N = 129 on the third day. Contact-angle data was statistically tested to reveal if there were any differences between the left and right side. This was done in R version 4.3.1 by using a two-sided Student's t-test, the significance level was set to $\alpha = 0.05$. All drop-morphology parameters are presented as the mean ± standard deviation. For the determination of the drop heights, N = 89 drops were measured on the first, N = 77 on the second, and N = 120 on the third day. Measurements were performed manually using Fiji software (ImageJ. 1.54f [48]). The height was measured at the highest point of the drop.

2.3 Analysis of cells

2.3.1 Cell-death measurement

The number of living and dead cells in the bioink was assessed directly before and after printing and was counted after using Trypan Blue Stain. Trypan Blue is a widely used dye that is only absorbed by cells with damaged cell membranes, but not by healthy viable cells. For the post-printing calculation, a cellular bioink was prepared, and pumped through the system. The cells were collected from the printing head in air (under the same conditions as during printing) but did not make any contact to the biopaper. Instead, they were collected in a tube. The volume of the collected bioink was 10 µl. The cells were immediately manually counted after trypan blue staining (addition of 90 µl trypan blue solution) using a CKX53 microscope (Olympus, Shinjuku, Tokyo, Japan) and a CAch N 10x/0.25 iPC objective. The cells that contained the stain, and thus appeared dark blue, were counted as dead cells.

2.3.2 Proliferation assay

Procedure for printed cells: All slides with printed fibrin hydrogel droplets were placed in 10 cm Petri dishes with 18 ml of supplemented DMEM at 37 °C. The slides were fixed within 1–3 h after printing (d 0), 24 h after printing (d 1), or 96 h after printing (d 4). Slides were gently washed twice with 1x PBS, and fixed for 20 minutes in cold 4% PFA. A DAPI-containing mounting medium - ROTI Mount FluorCare - was used to stain nuclei. Images were taken with an IX83 inverted imaging system equipped with a DP80 camera (Olympus, Shinjuku, Tokyo, Japan) either by using a UPlanFL N 4x/0.13, a UPlanSApo 10x/0.40, a UPlanSApo 20x/0.75, or a UPlanSApo 40x/0.95 objective. The adjustment of brightness, contrast, and size measurements were performed using cellSens Dimension software version 1.18 (Olympus).

Procedure for non-printed cells: Five drops with 6×10^6 HEK293H cells à 5 µl were pipetted into a floor of a glass well plate (P06G-1.5-20-F, MatTek Corporation, USA). To follow the same workflow as for the printing process, the floors of the glass wells were coated with fibrinogen (as described for the printing process) and as a control with PLL (0.1 mg/ml aqueous solution). The experiment was carried out n = 3 times. The proliferation of HEK293H cells was monitored over 4 days under six growth conditions. Four growth experiments were done in the fibrinogen surface for: 1) cellular bioink used in printing experiments, 2) cellular bioink without $CaCl_2$, 3) cellular bioink without thrombin, 4) cells in supplemented DMEM, 5) as a positive control, cellular bioink on a PLL surface, and 6) as a negative control, cells in supplemented DMEM on a PLL surface. Phase-contrast images were captured at 10x magnification every 30 minutes for 4 days using Incucyte® S3 (Sartorius AG, Germany).

2.3.3 Cell Morphology

HEK293H cells were transfected using PEI transfection (polyethylenimine, Polysciences, Warrington, PA, U.S.A.) with pEGFP-N1-plasmid (Clontech Laboratories, Japan). Therefore, 0.5 µg Plasmid-DNA per T75 flask with 40% cell density (~3 x 10^6 cells) was used. The DNA was mixed with 50 µl of serum-free DMEM. In a second tube, 0.5 µg PEI was added to 50 µl serum-free medium. Both tubes were mixed, incubated for 30 min at RT and added to the cells. Cells were continued 18 h after transfection for printing. Further bioink preparation and the printing procedure were performed in the same manner as for non-transfected cells. One day after printing, the slides were fixed and stained with DAPI, analogous to the proliferation assay.

For confocal-image acquisition, an inverted confocal laser scanning FV3000 microscope was used. EGFP-transfected samples were imaged by using a 4x objective (air immersion, 0.16 NA, to capture the whole drop), 20x (air immersion, 0.8 NA, to image a part of the drop), and 60x (silicon oil immersion, 1.3 NA, to image single cells). Olympus FLUOVIEW FV31S- software was used to operate the device and capture the images. The images were deconvoluted by using the Fiji plugins PSF Generator Version 1.1.1.2[31] and DeconvoluationLab2 Version 2.1.2[32], both developed by the Biomedical Imaging Group of the EPFL, Switzerland. Inside the PSF Generator, the Born & Wolf 3D Optical Model was used to generate a suitable point spread function (PSF), which was then further used to deconvolve the microscopic images in DeconvoluationLab2 with the Richardson-Lucy algorithm. If not stated otherwise, maximum projections of Z-stacks are presented.

2.4. Statistical analysis

Quantification of cell proliferation was performed by counting cells in four regions of interest (ROI) per droplet. Each ROI had an area of 29 834 µm^2. All ROIs were located within a distance of 100 µm from both the X- and Y-axis, whereas the geometrical origin of coordinate axes was located in the optical center of the droplet, see Figure S3. ROIs were defined to fit into the smallest droplet size. Overall, the statistical analysis was carried out for n = 3 independent experiments. For d 0: N = 44, for d 1: N = 39 and for d 4: N = 34 drops were analyzed. Images and quantification were performed via an Olympus IX83 microscope with the use of cellSens Dimension 1.18 (Build 16686) software, and statistical analysis via Prism GraphPad 9.4.3 (673). A non-parametric Mann-Whitney t-test showed a higher cell number on d 4 compared to d 0 and d 1 ($p<0.0001$).

2.5. Characterization of the fibrin hydrogel

2.5.1 Scanning electron microscopy

Printed samples on glass squares cut from a glass slide (1×1 cm^2) were prepared and gradually dehydrated one day before measurement using a series of ethanol:water solutions of increasing alcohol concentration % (v/v): 30, 50, 70, 80, 90, and 100. Then, a HMDS:ethanol (1:1 v) solution followed by pure HMDS were applied. Each washing step lasted for 15 minutes, during which a gentle circular motion was applied to the samples from time to time. Finally, they were left until the next day in a dry container with a moisture level below 30%. Before the imaging, a thin layer of gold (10 nm) was deposited by gold sputtering (BAL-TEC SCD 005 sputter coater, Lichtenstein), and the samples were mounted on SEM specimen stubs. Imaging was carried out using a Hitachi S-3200N scanning electron microscope (Germany) with the BSE (Robinson) detector, DISS scanning (Digital Image Scanning System, Point electronic Germany) and image processing DIPS (Digital Image Processing System. Point Electronic Germany) programs. For imaging of the printed acellular fibrin drops, the applied voltage was 20 kV, and 10 kV for the drops containing cells.

2.5.2. Polarization modulation infrared reflection absorption spectroscopy (PM IRRAS)

PM IRRA spectra with a resolution of 4 cm^{-1} were recorded using a Vertex 70 spectrometer with a photoelastic modulator (f = 50 kHz; PMA 50, Bruker, Germany) and a demodulator (Hinds Instruments, USA). A home-made glass cell for spectroscopic experiments was washed in water, then ethanol solution, and dried in an oven at 60 °C. The spectra were recorded from a stratified system composed of an optical window (CaF_2), electrolyte solution, fibrinogen/fibrin film, and Au substrate, reflecting the IR light. After rinsing the CaF_2 optical window with water and ethanol, it was cleaned using an UV ozone chamber (Bioforce Nanosciences, USA) for 10 minutes. A polycrystalline gold disc substrate (dia. 15 mm, Alfa Aesar, Germany), covered by a fibrinogen film, was fibrin assembled into the spectroelectrochemical cell. A bioink solution without the cell load was dropped onto the Au disk, whereby a fibrin gel formed immediately. The electrolyte solution was 0.01 M phosphate buffer solution in D_2O, pD = 7.4. For the analysis of the amide I mode in the protein, the half-wave retardation was set to 1600 cm^{-1}. The angle of incidence of the incoming IR radiation was 55° and the thickness of the electrolyte layer between the CaF_2 prism and Au electrode was approximately 4 µm. The spectra were measured over 7 days. Each measurement contained 400 averaged scans. The analysis of PM IRRA spectra was carried out using the OPUS v 5.5 software (Bruker, Germany). The qualitative and quantitative analysis of the secondary structure elements of fibrin gel on the gold electrode was carried out after background correction and normalization of spectra.

3. Results and Discussion

To characterize a new bioprinting technique, the measurement of the number of the printed living/dead cells, cell loss due to the printing procedure, cell viability, definition of the printing resolution, accuracy, and reproducibility, are essential. These parameters define printing properties. Characterization of printing techniques includes post-printing studies of both the cells, and the hydrogel matrix encapsulating the printed cells. The post-printing characteristics include studies of the cell behavior, cell migration, aggregation, spreading, and proliferation. The printed cells are encapsulated into a hydrogel matrix that provides stability and support for the printed structure, but it must display a certain flexibility and, elasticity, and be biodegradable; Therefore, describing the post-printing characteristics of the hydrogel is as essential as the post-printing characterization of the cells. Below, the overall characterization of the pneumatic conveying printing is described and compared to the characteristics of other inkjet bioprinting techniques.

3.1 Printing characteristics of the pneumatic conveying printing technique

The formulation of the bioink and the printing process may stress, and even damage the cells.[41] Therefore, it is first important to determine the number of dead cells, the cell loss, and the cell viability of the printed cells. First, we determined the number of dead HEK293H cells, due to bioink formulation and pneumatic conveying printing experiments, by staining with trypan blue. Trypan blue cannot be absorbed by living cells. Dead or perforated cells, on the other hand, will take up the substance and become dark blue in color as a result. A freshly formulated bioink contained $5.37 \times 10^6 \pm 0.46 \times 10^6$ HEK293H cells/ml and of these $0.24 \times 10^6 \pm 0.12 \times 10^6$ cells/ml were dead. The bioink dispensed from the printing head with a mounted needle was collected to establish the cell loss and viability change during the printing process. The cell number decreased to $4.78 \times 10^6 \pm 0.22 \times 10^6$ cells/ml and among them $0.34 \times 10^6 \pm 0.23 \times 10^6$ /ml were dead. The percent of dead cells was $5 \pm 2\%$ for unprinted and $7 \pm 4\%$ for printed. In an independent experiment, the needle was removed from the printing head and the number of living and dead cells passing the printing device was determined. In this way the effect of shear stress on the printing performance of the pneumatic conveying printing was elucidated. The percent of the dead cells coming through the pump to the printing head after removal of the needle was 5 ± 2 % and was the same as the percentage of normally treated cells. Thus, shear stress due to cutting of the bioink droplet in a stream of gas is responsible for the observed increase in the number of dead cells by ca. 2.-3%, indicating that 97-98% of cells are not affected by the shear stress. Wang et al studied the effect of shear stress on the viability of Chinese hamster ovary cells collected during thermal inkjet printing experiments.[49] The printing frequency, amplitude and time of the voltage impulse applied to produce the bubble and eject a drop were shown to affect the viability of cells, which in these experiments varied between 70 % and 95%. Bleaser at al found that in piezoelectric printing experiments, the viability of L929 mouse fibroblasts was 91 % and 76 % for shear stress of 5-10 kPa and above 10 kPs, respectively.[11] Reduction of shear stress acting on the cells during inkjet printing is a large experimental challenge.[11; 19; 49] In the pneumatic conveying printing technique, the shear stress on cells is low, ensuring mild printing conditions and high cell survival rate of the printed cells. Printing experiments displayed ca. 10% loss of the number of cells, compared to their content in a freshly f. It is most likely due to their adhesion onto the pipes of the pump syringe.[11; 31; 36; 47; 50; 51]

Next, we performed analysis of the shape and size of the printed droplets allowing the description of the resolution, and reproducibility of printing. A drop of bioink dispensed from the nozzle (radius of the drop at the nozzle, R_d), changes its dimensions after spreading on the surface of the fibrinogen biopaper (radius of the printed drop, R_p), forming a printed fibrin drop. The printed drops have an almost round shape, with an average vertical diameter of 1260 ± 259 µm and a horizontal diameter of 1254 ± 285 µm, see Table S1. Assuming a spherical shape of the printed drops, the average radius of the printed drop $R_p = 628 \pm 136$ µm and is almost twice as large as the radius of the drop dispensed in air from the needle ($R_d = 345$ µm). The initial volume of the drop, the surface pressure of the bioink, the line tension of the liquid-solid-gas boundary, as well as kinetics of the hydrogel formation are the factors that determine the final shape of the printed drops and thus the resolution of the printing. For comparison with the printing results, the Sessile drop contact angles of acellular and cell-loaded bioink (macroscopic drop, volume of 12 µl) were measured and are listed in Table 1.

The values of the macroscopic contact angles (Sessile drop measurements) of the bioink drop-forming fibrin hydrogel on the fibrinogen surface depended on the presence of the cells in the solution. An increase in the contact angle of the cellular bioink is the consequence of the lowering of the surface energy of the bioink containing HEK293H cells, see Table 1. Fibrin is characterized by a water contact angle of 60 – 75°.[52] Contact angles of the bioink liquids are larger than the water contact angles, and may be related to the bioink composition and thus surface energy.

Table 1. The surface energy (γ), volume (V), radius at the nozzle (R_d), and bioink contact angles (θ_{bioink}) of the cell-free and cell-loaded macroscopic (Sessile drop) and pneumatic conveying printing bioink drops deposited on the fibrinogen-coated glass surface.

Bioink: DMEM + Thrombin + $CaCl_2$	γ [mN/m]	**Sessile drop**			**Printed drop**		
		V [µl]	R_d [µm]	θ_{bioink} [°]	V [µl]	R_d [µm]	θ_{bioink} [°]
No cells	72.6 ± 1.8	12	1420	84 ± 10	0.172 ± 0.018	345 ± 36	40 ± 7
6 x 10^6 HEK293H/ml	58.5 ± 4.0	12	1420	91 ± 6	0.172 ± 0.018	345 ± 36	41 ± 8

Contact angles measured for drops formed during pneumatic conveying printing exhibit distinct characteristics. As listed in Table 1, the contact angles (~40°) are lower than for the Sessile drops, and their values do not depend on the bioink composition, indicating that the spreading of these drops depends on other factors than the surface energy of the bioink and fibrinogen. Line tension arises when a droplet lens contributes to the total surface energy of a three-phase system, and therefore affects the values of measured contact angles.[53-55] The observed decrease in the contact angle of the printed drops compared to the Young contact angle indicates an expansion of the three-phase contact line and a fast-spreading (wetting) of the surface by the bioink. The spreading ability of the bioink drops may be further affected by the kinetics of the fibrinogen polymerization and the force of collision of a drop brought to the surface in a gas stream. Note that the velocity of an ejected bioink drop (~ 0.2 m/s) is low. Collision of a slowly moving drop with a surface will not lead to a large deformation of the drop. In the printing experiment, a bioink drop contacts and spreads on a soft protein coating (fibrinogen) [29], which absorbs a large portion of the collision energy [51]. Low values of the measured contact angles (see Table 1) confirm that the bioink droplets penetrate into the biopaper. Clearly, the properties of the bioink and the biopaper are responsible for an increase in the size of the printed drop, lowering the printing resolution to ca. 1000 µm. The printing procedure is, however, protective for the cells, as the low number of dead cells and high cell viability confirm.

Knowing the θ_{bioink} and the R_p = 628 ± 136 µm of the printed drops, the radius of curvature ($\tilde{R}_p$) of a spherical drop was calculated. $\tilde{R}_p$ equals 956 µm, indicating that the expected drop height is ~330 µm and the printed drop has a volume of 158 nl. The mean measured height of the printed drops is 300 µm ± 30 µm, see Figure S2 in Section S3 and Table S3 in Section S4. The volume of the printed drop, calculated from its geometry (158 nl) agrees well with the volume of the dispensed bioink (172 ± 18 nl). Thus, the printing does not lead to losses of the bioink and indicates that no satellite drops are formed during the printing process, indicating that the printing technique is accurate.

Another important parameter characterizing the printing technique is the distribution of cells inside freshly printed drops. Figure 2 shows confocal fluorescence images of HEK293H cells 2 h after printing (d 0). The printed droplet is roundish with a well-defined boundary between the fibrin hydrogel and fibrinogen biopaper as seen in the optical microscopy image in Figure 2B.

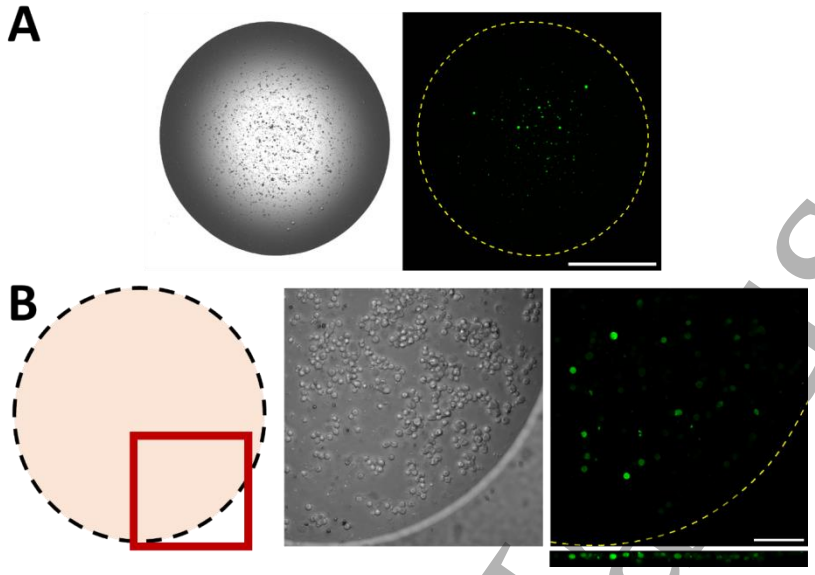

Figure 2. Representative confocal microscopy images of printed drops containing HEK293H cells in fibrin hydrogel. **A:** Whole drop. Left panel: Signal from the transmitted-light (TD) channel; the drop shape is visible. Right panel: Signal from the EGFP-channel, green spots are HEK293H cells. The dotted line marks the border of the drop. The XY-plane is shown. Scale bar = 500 µm. Images were taken 2 h after printing **B:** Fragment of a drop, as shown in the left panel. Middle panel: Signal from TD-channel, the drop border, and location of many cells are visible. Right panel: Signal from the EGFP-fluorescence channel; green spots are HEK293H cells. The dotted line marks the border of the drop. The EGFP-signal is divided into the XY-plane (with the dotted line) and the projection of a Z-stack from a part of one drop in the XZ-plane (narrow panel below, the Z-dimension is 30 µm in height). Scale bar = 100 µm. Note: Images (A) and (B) are from different drops.

The HEK293H cells were randomly distributed in X- and Y-planes inside the droplet. The highest content of the cells is expected in the middle of the drop, at its maximum height. Figures 2 and 3 show that the cells are unevenly distributed over the drop surface, and the cell content decreases at the edges of the drops (Figures 2,3 A). In addition to the distribution analysis of the cells in the droplet, we transfected the cells with EGFP before printing. These cells are clearly visible 2 h after printing, however not all cells were transfected (Figure 2 A,B). This presents an advantage in terms of cell count, as it allows us to microscopically analyze individual cells more effectively. The EGFP transfection can now be used for further morphological analyses over a longer period of time, to study the behavior of the cells in the droplet. From the XY-perspective, the cells are rounded, with an average diameter of 12.5 ± 2.5 µm, a size that is characteristic of HEK293H cells.[56] The XZ-perspective [Figure 2B (right panel, EGFP signal)] shows that in a printed drop, the cells lie next to parallel planes. Based on these studies, we conclude that HEK293H cells show a typical morphology 2 h after printing (Figure. 2 B), indicating that the printing procedure causes no stress which could be expressed in the cell morphology.

3.2 Post-printing characterization of the pneumatic conveying printing technique

Knowing that the printed HEK293H cells main their typical morphology we followed the cell proliferation process over few days after printing.

Cell proliferation. We examined cell proliferation over 4 days after printing. To count the cells, we first stained them with DAPI. The nuclear staining simplified cell counting and also showed intact nuclei. The cell nuclei at d 0 (Figure 3A, d 0) showed homogeneous DAPI staining. No fragmentation of the cell nucleus, i.e. incipient apoptosis, was recognizable. Again, this result indicates that the printing procedure is mild for cells and does not cause visible damage to the cells. Images of different droplets were taken under a brightfield and fluorescence microscope for samples incubated for d 0 (1 h after printing), d 1 (24 h), and d 4 (96 h), and are shown in Figure 3.

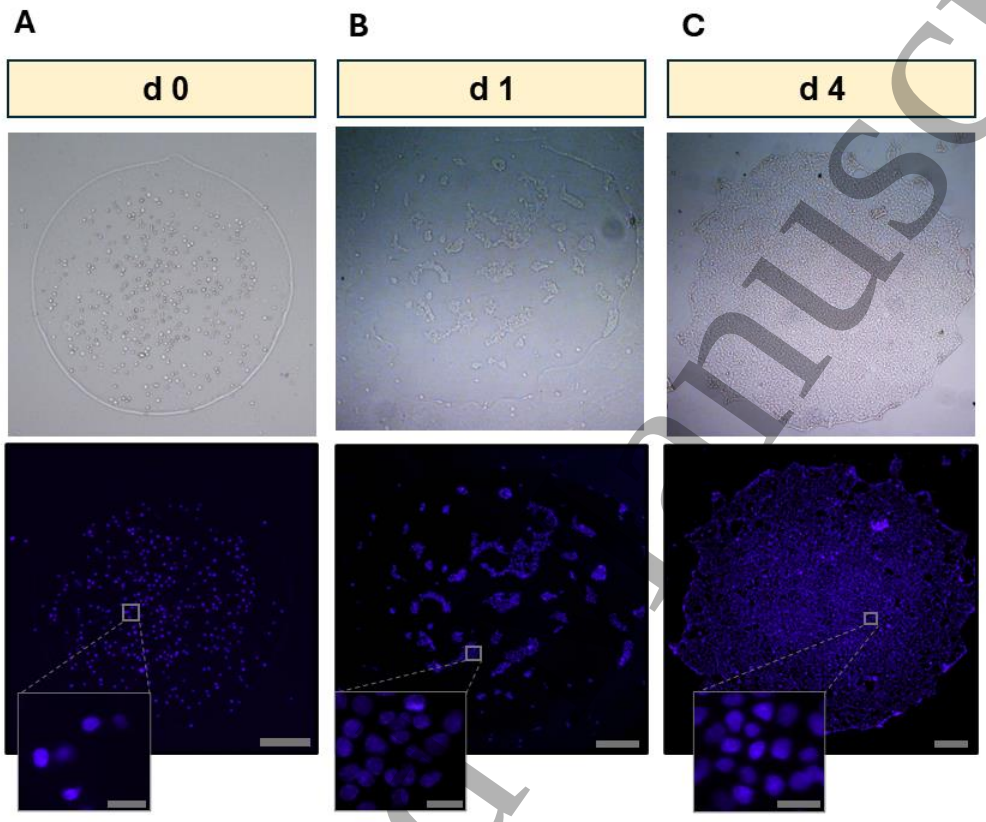

Figure 3. Proliferation of HEK293H cells in printed droplets over time A: d 0; B: d 1 and C: d 4. Upper panel shows bright-field microscopy and the lower panel shows fluorescence microscopy, DAPI staining of printed drops. Images for each time point illustrate a different droplet. Scale bar: 200 µm. Insets: Close-ups of the cell nuclei, Scale bar: 20 µm.

One hour after printing (d 0), a well-defined droplet, unevenly filled with round cells, was observed and is shown in Figure 3A. The printed drop has a smooth round shape and is clearly visible in the optical microscopy image. Overall, at d 0, an average number of 21 ± 18 cells per ROI was counted (see Figures 4 and S3). Knowing the vertical and horizontal diameter of the printed drops and their average area of 1.27 ± 0.51 mm^2, an average number of 978 ± 1042 HEK293H cells per drop was calculated, see Table S4 in Section S5. The large standard deviation is due to two factors. First, in each drop, the cells were distributed unevenly and displayed a concentration gradient from the middle of the drop (top, largest height) to the border (lowest height), which was cell-free. That is consistent with the drop shape, and the presence of a large number of cells in the center of the drop that is higher than at the edges. In the vicinity of the drop edge, the number of cells is very low, suggesting that the thickness and/or structure of the fibrin at the drop border is not favorable for the incorporation of cells. Second, there were outliers, such as droplets with few or no cells, or with a higher-than-average number of cells, possibly due to cell sedimentation or adsorption in the pipes of the printer. These two factors are responsible for the large standard deviation value. Based on the printing data,

16.7 µl of the bioink was used per sample, producing 97 droplets, and, knowing the cell concentration, the average theoretical number of cells in the droplets of 1043 ± 90 was calculated. The results of the theoretical and the experimental values correlate well with each other. The experimental value was lower, being 93.5% of the theoretical one, corresponding well with the cell loss established in this study (7.8% during the bioink formulation and printing).

On d 1, the morphology of the drop and the distribution of cells within the drop changed, see Figure 3B. The drop developed a serrated edge and its borderline was less pronounced in the optical microcopy image. The fibrin hydrogel was present within the drop, but changed its morphology and structure, as described below in paragraph 3.3. Within the drop, the cells migrated to form aggregates. Quantitative analysis indicates that over the first 24 h, the number of cells equaled 21 ± 19 cells per ROI, see Figure 4. It was calculated to be 1238 ± 1522 cells per droplet, see Table S4. No increase in the number of cells was observed 24h after printing, indicating that the cells experience some stress which inhibits their proliferation.

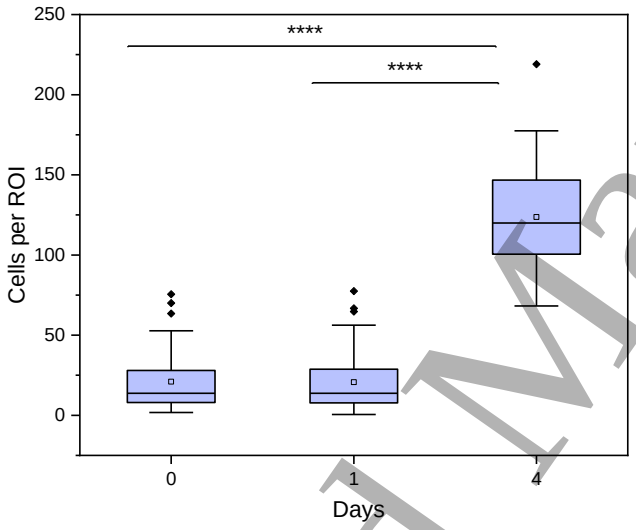

Figure 4. Post-printing quantification of cell numbers. Proliferation of HEK293H cells over a 4-day period; samples were from at least three independent printing procedures. ROI number: d 0: N=44, mean = 21.02, SD = 18.03, d 1: N=39, mean = 20.64, SD = 19.06, d 4: N=34, mean = 123.74, SD = 34.37. **** $p<0.0001$.

On d 4 the printed drops are clearly seen in the optical microscopy image, indicating that the fibrin hydrogel is present on the biopaper surface and provides support for the printed HEK293H cells. The drop is filled with cells and its border line is clearly visible in the optical microscopy image shown in Figure 3C. The drop developed further serrated edge pointing on an increase in the elasticity of fibrin fibers to accumulate increasing number of cells. The cells covered the imaged area of the droplets, with nearly 100% confluency (Figure 3 C). The distribution of cells is equal over the entire surface, including the drop edges. The average number of HEK293H cells in 4ROIs per drop increased to 124 ± 34, corresponding to 11773 ± 7691 cells per droplet (Figure 4); see Table S4. On d 4 the increase in the cell number reached 1200%. The doubling time of the HEK293H cell line is between 24 and 45 h, with an average of 30 h under normal conditions in the 2D cell culture flask.[57]. Considering, that over the first 24 h after printing we observe a lag time in proliferation, it is expected that after 72 h (end of d 4) the number of cells increases by 1100%. Our experimental value agrees well with the theoretical prediction indicating that the initial number of living cells was determined correctly.

The post-printing monitoring of the cells displayed a lag time of approximately 24 h before proliferation started. This lag phase is connected with the mobility, migration, and agglomeration of cells. In this phase, the cells preserve their roundish shape and over time start to adhere to the surface of the biopaper (fibrin). Several factors might be responsible for the observed cell behavior: (i) the high concentration of Ca^{+2} (in total 41.8 mM $CaCl_2$), (ii) the presence of thrombin, (iii) the 3-D structure of the fibrin hydrogel, (iv) interactions between the fibrin coating and the cells, or (v) long-lasting post-printing stress of cells requiring their recovery (e.g., lesions in the membrane after collision with the substrate). First of all, unphysiologically high levels of Ca^{2+} suggest that the bioink solution may be hypertonic for the cells impairing for example cell-cell communication. In general, Ca^{2+} play a pivotal role in numerous cellular processes, acting as a second messenger in signal transduction and a regulator of various cellular activities. While physiological extracellular Ca^{2+} concentrations are tightly regulated around 1.1–1.3 mM, elevated levels can have profound effects on cell communication and function.[58] For example, Ca^{2+} affects the function of gap junctions, which are critical for direct cell-to-cell communication. Excessive extracellular Ca^{2+} concentration can alter connexin expression or function, potentially disrupting the synchronized activity of cells in tissues such as the heart and nervous system.[59] Ca^{2+} is also a critical modulator of cell cycle progression and differentiation. High extracellular calcium can trigger aberrant growth patterns in certain cell types.[60] Also, Ca^{2+} may promote apoptosis by altering mitochondrial permeability and initiating caspase-dependent pathways. Furthermore, Ca^{2+} influences the organization and stability of the cytoskeleton. Elevated levels can disrupt cytoskeletal dynamics, impairing processes such as cell migration and adhesion, which are crucial for tissue repair and immune responses.[61] Moreover, depending on its concentration, thrombin induces various effects on different cell types.[62] For example, thrombin influences proliferation, or the stabilization of cell-cell contacts particularly in pathological processes [63] and therefore would be rather expected to facilitate proliferation than slow it down. At the moment, it cannot be ruled out that the addition of thrombin influences the time delay in the proliferation of HEK293H cells.[23; 64-66] Furthermore, it cannot be excluded that calcium and thrombin influence each other. Further investigations are required to clarify these cellular processes in the first 24 h. It is well known that cells survive and proliferate in fibrin gels, and control experiments we tested the effect of the biopaper coating: the structure, morphology, and elasticity of fibrin fibers on the behavior of HEK293H cells. The observed delay in the proliferation of HEK293H cells may also be a consequence of printing stress. To test the possible reasons for the observed delay in proliferation, control experiments on not-printed cells were carried out.

Different growth conditions were tested to gain information about the proliferation of printed HEK293H cells by pipetting 5 µl of cells containing liquids onto the fibrinogen-coated surface from (i) bioink, (ii) bioink without $CaCl_2$, (iii) bioink without thrombin, and (iv) DMEM (without $CaCl_2$ and thrombin). The second set of proliferation experiments was carried out on PLL-coated substrates with bioink as a positive control and DMEM as a negative control. Under all tested conditions, the cells showed proliferation, and the population was nearly 100% confluent before the experiment ended after 96 h (d 4). Figure 5 shows a time series of optical microscope images of HEK293H cells growing under different conditions.

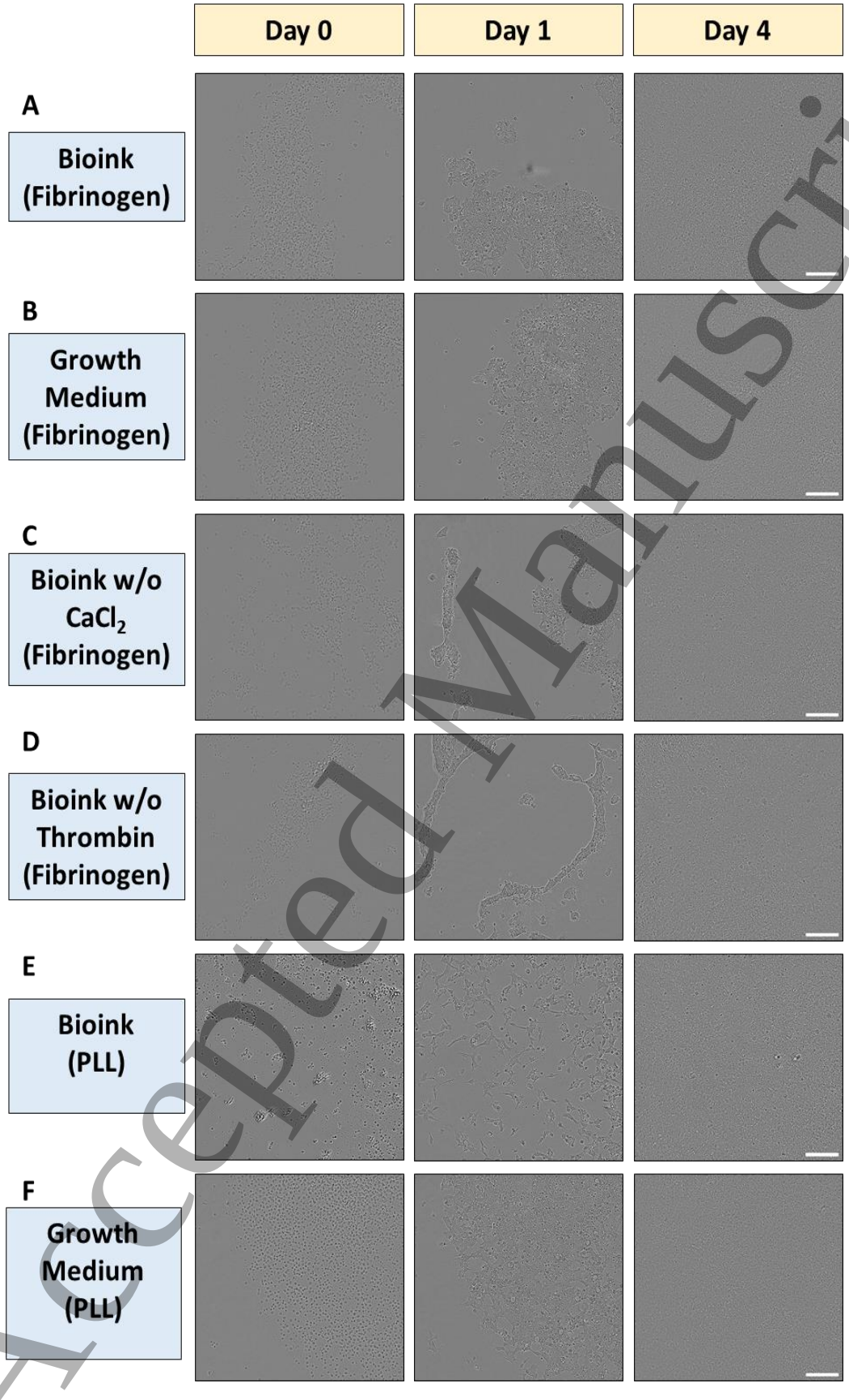

Figure 5: Time series (d 0 = after 1 h, d 1 = after 25 h, d 4 = after 97 h) optical microscopy images of HEK293H cells pipetted under different conditions: **A**: fibrinogen coating cells in bioink (upper panel); **B**: fibrinogen coating cells in supplemented DMEM (growth medium, middle panel); **C**: fibrinogen coating cells in bioink without $CaCl_2$; **D**: fibrinogen coating cells in bioink without thrombin; **E**: polylysine coating in bioink and **F**: polylysine coating in a supplemented DMEM (bottom panel). Representative images from the n = 3 repetitions of the experiment were chosen. Scale bars = 200 µm.

In all cases, the freshly deposited cells (d 0, 1 h) covered the surface evenly, and had a rounded morphology. The first 24 h displayed differences in the distribution and shape of the cells exposed to fibrinogen and PLL substrates (Figure 5). On the PLL substrate, already a few hours after deposition, the HEK293H cells displayed a non-circular morphology, indicating interactions and adhesion to the substrate. For populations growing on PLL, proliferation started during the first 24 h of the experiment (d 0, see Figure 5E), yielding a surface homogenously covered by the cells. On the PLL substrate, no differences in the morphology and proliferation of HEK293H cells were detected between the cells present in the bioink and DMEM (Figures 5E-F). This result does not confirm our hypothesis suggesting that the high concentration of Ca^{2+} may cause stress and affect the spreading, adhesion, and proliferation of HEK293H cells.

On all investigated fibrin (when exposed to bioink solution) /fibrinogen (when exposed to DMEM) substrates, initially uniformly distributed cells started to migrate and aggregate over the first 24 h of the experiment, producing an unevenly covered surface (Figure 5A-D). The cells were densely packed into elongated, interconnected band-like structures, with well-defined edges that are similar to structures observed in printing experiments (see also Figure 3B). The elongated cellular structures moved across the surface, sometimes they disappeared from the region of the image capture. On the fibrin surface, the migration of cells started earliest (6–12 h) in the growth medium, followed by the bioink (12–18 h) and bioink without Ca^{2+} and without thrombin (18–24 h). Under the above listed conditions, during the first 24 h, the cells preserved their rounded shape. We observed that the cells migrated and began to aggregate. In these experiments, we confirm that the bioink had a negligible effect on the ability of HEK293H cells to migrate, aggregate, and proliferate. At the end of d 2 (36–48 h), the four populations growing on the fibrin/fibrinogen coatings finally started to proliferate. The edges of the cellular aggregates were preserved, unlike in control populations growing on the entire surface of the PLL coating. At d 3, the cell morphology changed to non-circular and they spread, covering the fibrin/fibrinogen surface with nearly 100% confluency (Figure 5A-D). Regardless of whether HEK293H cells were printed or pipetted onto the fibrinogen-coated surface, we observed a 24 h lag time in cell proliferation, preceded by intensive cell migration and aggregation. This experiment excludes our hypothesis of the effect of printing caused a long-lasting stress in cell proliferation. Summarizing our results, we conclude that the fibrin/fibrinogen substrates induced the cell migration and aggregation that delayed cell proliferation by approximately 24 h, a phenomenon that was not specific to pneumatic conveying printing and was not observed on the PLL coating.

3.3 Morphology and structure of the printed fibrin hydrogel

HEK293H cells need time to acclimate to the new environment of the protein coating. To understand the post-printing processes, we investigated the morphology and structure of the fibrin coatings created during the printing experiments.

Structural changes in the fibrin hydrogel printed from the cellular bioink were observed using SEM (Figure 6). Directly after printing, well-defined drops of the hydrogel-encapsulating cells were visible in the SEM image (Figure 6A). Spherical cells were found within the drop. The drop border, made of a thick fibrin film, was cell-free, confirming results described above (Figures 2, 3A).

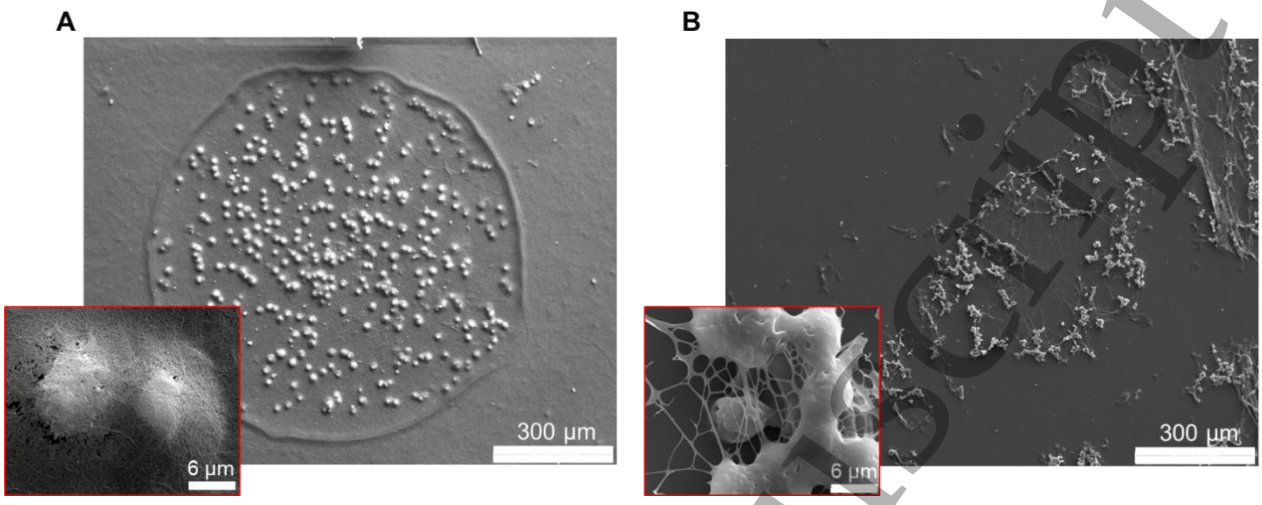

Figure 6. Post-printing microstructure images of fibrin hydrogel droplets with a cell load. SEM micrographs of **A:** 1-3 h after printing (d 0), and **B:** d 1 24 h fibrin gel printed from a bioink containing 6×10^6 HEK293H cells/ml using pneumatic conveying printing technique on a fibrinogen-coated biopaper. The insets in A and B show a high-resolution image from the droplet.

As shown in the inset of Figure 6A, directly after printing, interconnected, branched fibrin fibers completely coated the spherical HEK293H cells. This fibrin coating underwent large morphological changes 24 h after printing and as shown in Figure 6 the fibrin fibers were significantly thinner, and almost invisible in the SEM image. The inset in Figure 6B clearly shows 3D cell aggregates encapsulated in a stretched fibrin-polymer scaffold. The fibrin network changed, yielding long, thin, and stretched fibers that still held cells in the droplet shape. The thinning of the fibrin film was due to its stretching, caused by cell migration and aggregation as well as biopolymer biodegradation.[33; 67] The cells migrated and aggregated, preserved their spherical shape, and were present within the drop area, confirming that the fibrin hydrogel give and supports the structure of the printed features. Before the experiment, the sample had been stored in DMEM, thus any drying of fibrin hydrogel and encapsulated in the drop cells is excluded. For samples stored for longer than 24 h, no stable SEM images were obtained. The drying procedure of the sample prior to SEM experiments destabilized the printed structure.

To test a possible effect of cells on the fibrin biodegradation, the hydrogel was printed from an acellular bioink. The SEM images in Figure 7 show that fibrinogen adsorbed on the glass surface reacted with thrombin delivered in the bioink, yielding fibrin biopolymer droplets.

The average size of the drops printed from a cell-free bioink was comparable to the size of the drops printed with HEK293H cells. The inside of the droplet was rather uniform, while its edges displayed a more complex structure (Figure 7). Insets in Figure 7A show that the fibrin formed a net of densely packed, highly branched, interconnected fibers. The average length of the printed fibrin fibers was 3.6 ± 2.0 µm and the diameter 86 ± 29 nm, see Figure S5 and Table S5 in Section S7).

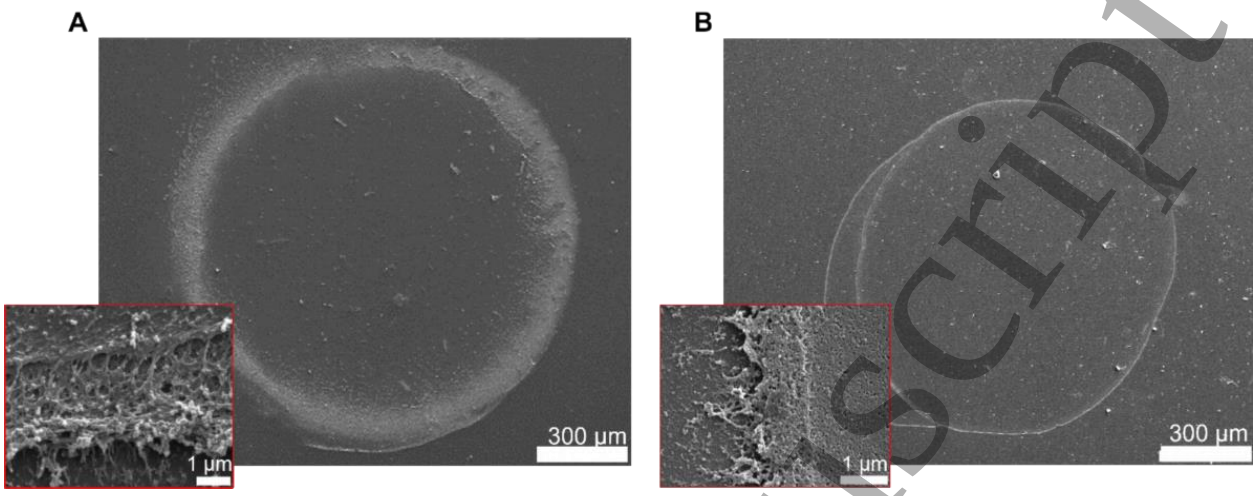

Figure 7. Post-printing microstructure images of fibrin hydrogel droplets. SEM micrographs of fibrin gel printed using the pneumatic conveying printing technique on a fibrinogen-coated biopaper captured at **A:** d 0 and **B:** d 7. The insets in A and B show a high-resolution image of the edge of the droplet.

Fibrin fibers formed in aqueous solutions are usually 1 – 10 µm long with a diameter of 30 – 400 nm [29; 67-72], (Table S5), indicating that fibrin fibers formed during the bioprinting experiments have comparable dimensions to fibers formed in the solution phase.[27; 30] Fibrin printed using a pneumatic conveying technique has a porous microstructure characteristic of hydrogels (Figure S4). At the drop's edge, the fibrin structure changed; the fibers were densely packed, making a compact film. As revealed in Figure 7B, the fibrin drops kept their shape over 7 days of storage in 0.15 M NaCl (0.15 M) and 0.01 M $CaCl_2$ (0.01 M) in D_2O. A high-resolution SEM image shows a compact, poorly interconnected structure. The morphology and stability over time of the fibrin droplets printed from the acellular bioink (Figure 7B) differs significantly from the one observed for droplets printed from the cellular bioink (Figure 6B), suggesting that the cells may to affect the structure of fibrin hydrogel.[73; 74]

To understand molecular-scale changes taking place in fibrin, *in situ* PM IRRAS experiments were performed over seven days. Figure 8 shows deconvoluted PM IRRA spectra of a fibrinogen film and fibrin formed on a gold surface. Due to the overlap of the water deformation mode with the amide I mode region, experiments were carried out in D_2O. The amide I and amide II vibrational bands measured in D_2O change their nomenclature to amide I' and amide II'.

PM IRRA spectra of fibrinogen (Figure 8A) and fibrin (Figure 8B-D) show three broad and asymmetric IR absorption modes. Deconvolution of the amide I' (predominantly C=O stretching mode) vibration mode provides information about the secondary structure of proteins.[75; 76] Deconvolution of the amide I' band of fibrinogen (before the reaction with thrombin) yielded five amide I' bands centered at: 1676, 1656, 1640, 1630, and 1612 cm^{-1}, reflecting the complex structure of the protein [77; 78], (Figure 8A and Table S6). The α-helices (gray band in Figure 8A), β-sheets (blue band) are the main structural elements of fibrinogen, agreeing with earlier literature reports.[78]

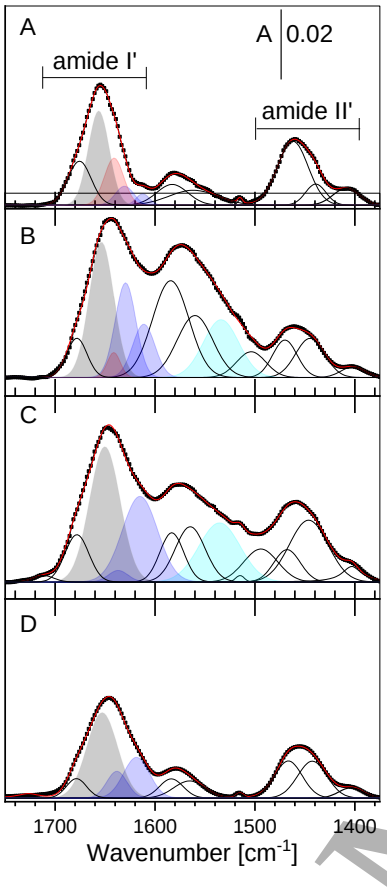

Figure 8. In situ infrared spectra of fibrinogen and fibrin hydrogel stored in 0.01 M phosphate buffer solution, pD = 7.0 in D_2O. Deconvoluted PM IRRA spectra of **A:** fibrinogen and B-D) fibrin gel on a polycrystalline Au surface recorded at **B:** d 1, **C:** d 6 and **D:** d 7. Shaded areas correspond to IR absorption modes described in the text: amide I' modes of α-helices (gray), β-sheets (blue), and random coils (red), and the IR absorption mode of D_2O (turquoise); A – absorbance.

The reaction of fibrinogen with thrombin led to the formation of fibrin and caused some changes in the amide I' mode and the protein structure. The α-helices remained the dominant structural element of fibrin.[77] Over time, the amide I' mode at 1640 cm^{-1} (red surface in Figure 8 B) vanished, evolving into stronger modes at lower wavenumbers that are characteristic for β-sheets and aggregated β-sheets (blue surface in Figure 8 B-D). The presence of aggregated β-sheets is a consequence of strong intra- and intermolecular interactions and the formation of fibers. Over 7 days, the shape and intensity of the amide I' band changed and became similar to the mode of fibrinogen. The most pronounced changes occurred in the 1600 – 1500 cm^{-1} spectral range (Figure 8). The IR absorption modes lying between the two amide modes have a complex origin and may be assigned to $\nu_{as}(COO^-)$, amide II (observed in H_2O), and D_2O water association modes.[75; 79] In the fibrin coating, a new IR absorption band appeared at 1533 cm^{-1} (cyan surface in Figure 8 B-D). D_2O has a weak combination band around 1550 cm^{-1} involving OD bending and overtones of librational modes.[80; 81] The dependence of this mode on hydrogen bonding has analytical value, and informs about different molecular environments.[82] In PM IRRAS, absorption modes of bulk water are strongly attenuated and contribute to the background spectrum. Thus, only D_2O molecules that were coordinated to fibrin had restricted rotation and therefore led to a down-shift of this combination mode. We propose that the absorption band at ~1530 cm^{-1} arose from water in the hydrogel that was coordinated to fibrin. A decrease in the intensity of this mode over time reflects the dehydration process of fibrin fibers that is so characteristic of hydrogel aging (biodegradation).

SEM and IR spectroscopy results indicate that the fibrin-biodegradation process starts with a loss of water, leading to fibrin structural shrinkage, which in turn facilitates extensive intermolecular interactions and conformational changes in the protein, yielding aggregated β-sheet structures. Fibrin printed from a cellular bioink underwent a faster biodegradation than the drops printed from an acellular bioink. The interaction with the cells, their migration, and their metabolites possibly affected the fibrin's elasticity and stability.

3.4 Performance of pneumatic conveying bioprinting compared to other inkjet bioprinting techniques

Pneumatic conveying printing is a new inkjet-drop-on-demand bioprinting technique that has very good printing characteristics compared to other inkjet printing techniques. Table 2 shows a comparison of inkjet bioprinting techniques and summarizes our results on pneumatic conveying printing.

Table 2. Characterization and properties of different inkjet bioprinting techniques.

Inkjet printing technique	**Mechanism**	**Impulse of the drop ejection**	**Nozzle diameter [µm]**	**Volume ejected drop**	**Concentration of cells [million / ml]**	**Cell viability [d 0]**	**Disadvantages**	**Ref.**
Pneumatic conveying	Ejection and deposition of a drop in a stream of gas	Continuous gas stream flow rate 50 -150 m/s	100-300	170 nl	6	93	- shear stress	This work
Piezoelectric	Use of piezoelectric actuators to squeeze and eject a drop	Voltage 45 - 200 V applied for 50-200 µs	80-200	30–150 nl	1–10	70–98	-pulsed pressure increase in the chamber -shear stress -clogging of the nozzle, -jetting velocity may damage the cell's membrane -droplet flight bending	[11; 18; 35; 43; 47; 83]
Thermal	Local heating to produce a hot bubble that ejects the bioink	Temperature 250 -300 °C applied for ~ 2µs	10-100	80–150 pl	1–6	~85	-shear stress -clogging of the nozzle, -jetting velocity may damage the cell's membrane -temperature rise -droplet flight bending	[41; 49-51; 84; 85]
Electrohydrodynamic jetting	Use of high voltage to produce drops from the Taylor cone	Voltage 1-20 kV to give electric field 0.5- 0.9 kV/ mm	15 -1000	10 pl–4 µl	1–5	70–90	- shear stress -clogging of a nozzle with a diameter < 50 µm -electroporation of cell membranes in electric field	[46; 86]
Intersecting jets, piezoelectric	Use of piezoelectric actuators to squeeze and eject a drop with a bioink and gelling agent, combining both drops	Voltage 60 - 120 V applied for 20-45 µs	120	Not reported	5	85	-shear stress -clogging of the nozzle, -jetting velocity may damage the cell's membrane	[36]

Inkjet printing techniques operate on different methods of drop-on-demand production and ejection. In piezoelectric and thermal inkjet printing the cells present in a bioink are exposed for short time to high pressure, reaching 10^6 Pa.[19; 34] Not only cells in the ejected droplets, but also the cells present in the ink in the chamber suffer from the pulsed pressure, indicating that some cells are exposed thousands of times to pulsed pressure before they are ejected and printed. In pneumatic conveying printing cells are not exposed to high pressure, indicating the operando modus of this technique is of large advantage in the field of inkjet printing technology. Shear stress arising during the drop ejection from the nozzle is a clear disadvantage of all inkjet bioprinting techniques.[2; 6; 11; 18; 19] In the case of the pneumatic conveying printing technique, the velocity of the gas at the contact surface with a liquid bioink squeezed from a pneumatic syringe is responsible for the appearance of the shear stress and possible damage to cells. Our results show that for a nozzle with an inner radius R_0 of 80 µm, the optimum velocity of gas flow is ~150 m/s. These rates of gas flow may be harmful to cells. It was demonstrated that the gas entrance velocity into medium containing cells causes damage to cells at a flow rate higher than 60 m/s.[87; 88] 97-98% of the cells survives the printing procedure indicating that the shear stress causes much less damage to the cells than in piezoelectric inkjet [11; 19] and thermal [49] inkjet printing. The velocity of a bioink drop approaching the biopaper surface is ~ 0.2 m/s, a speed that is not expected to cause damage to the cell membrane due to the collision force.[18; 47; 89] For example, in piezoelectric inkjet printing experiments, the jetting velocity of a bioink drop of 1.8 m/s had a negligible effect on the viability and membrane compactness of 3T3 fibroblasts.[47] We found that the percent of printed dead cells was only slightly higher compared to unprinted dead cells [unprinted cells (5 ± 2)% and printed cells (7 ± 4)%]. On d 0 (1–2 h after printing, time frame depending on the number of analyzed samples, no differences between 1 h and 2 h were observed) more than 93% of the cells present in the bioink were alive, indicating that the bioink extrusion and subsequent deposition in the gas flow on the substrate were gentle to the cells (Table 2).

Due to the fact that in pneumatic conveying printing cells are extruded from a pneumatic syringe, bioinks with high viscosity can be used without any clogging of the nozzle, a common disadvantage of other inkjet printing techniques (Table 2).[2; 6] Thus, elimination of the problem of nozzle clogging is one of the clear advantages of the pneumatic conveying printing technique, because both viscous and not-viscous liquids can be printed.[38; 45] It is a very unique property among inkjet printing techniques allowing for the use of inks with viscosity typical for extrusion based techniques.[90] The possibility to use of viscous liquids allows for the formulation of bioinks with biological cell loads (>10 million/ml). A large number of cells in a bioink leads to a decrease in the surface energy of the liquids, (Table 1) reducing the shear stress due to drop ejection and therefore reduces stress on the cells. For example, in inkjet printing experiments, surfactants (Pluronic acid) [91] or polymers (negro 2018) were added to a bioink to reduce the surface energy of the liquid and reduce the shear stress.

The ability of a drop to spread on the surface and the kinetics of hydrogel formation determine the resolution of pneumatic conveying printing. The resolution of printing HEK293H cells on the fibrinogen surface is quite low (ca. 1000 µm). For example, the printing of HEK293H cells from an alginate sol had a resolution of 400 µm. [38] Compared to other inkjet printing techniques, pneumatic conveying printing still has a rather poor resolution.[2; 6; 12; 90] The resolution of the pneumatic conveying printing technique depends primarily on the size and shape of the nozzle and its hydrophilicity. It was proved that its resolution varies between 100 and 1000 µm. [38; 45] For example a use of nozzles coated by hydrophobic films increases the resolution of the pneumatic conveying printing.[38] However, many of the hydrophobic nozzles are cytotoxic. To improve resolution, in the future work we plan to improve the resolution of pneumatic conveying bioprinting by using non-coated and silianized glass-capillary nozzles with diameters smaller than 100 µm. The rate of gelation reaction is another parameter that affects the resolution of pneumatic conveying printing technique. A challenge here is the search for biocompatible sols that undergo very fast gelation. Due to the fact that biological cell loads may be printed by pneumatic conveying bioprinting technique, it has potential as an application for printing organelles or models of tissues e.g. skin. For these purposes, its lower resolution, compared to other inkjet printing techniques, is not a disadvantage.

4. Conclusions

Results described in this manuscript demonstrate the applicability of the inkjet pneumatic conveying printing technique for cell-printing purposes. We demonstrated that pneumatic conveying printing offers several improvements over traditional inkjet printing technology, including gentle printing conditions, reduction of shear stress, high cell-survival rate, and applicability to viscous liquids with a biological cell content. The mechanism of the drop ejection is based on the cutting and deposition of a drop of bioink in a stream of gas. It differs from the mechanisms involving either application of a high voltage or temperature rise used in other inkjet printing technologies. The *modus operandi* of pneumatic conveying printing reduces the shear stress on the printed cells, as confirmed by the 93 % cell viability measured directly after printing. The technique is applicable to

viscous liquids, and in the future, it will be employed to print models of tissue (e.g., skin). Furthermore, the use of bioinks with high concentrations of cells reduces the surface energy of bioinks. It is a clear advantage of pneumatic conveying printing that improves the resolution of this technique.

During printing, we observed approximately 10% loss of cells compared to their concentration in the freshly formulated bioink. This is primarily associated with cell adhesion to the pipes and the syringe, as reported other inkjet printing experiments[92]. Further improvements in the printing performance, such as stirring the bioink solution, and using shorter pipes to deliver the bioink has been recently used to increase the printing efficiency.

The post-printing characterization shows that HEK293H cells start to proliferate in the fibrin drops after one day of lag time. Control experiments proved that the lag time in the proliferation of HEK293H cells is due to the chemical nature of the biopaper (fibrin hydrogel) and does not depend on the printing technique or the composition of the bioink. From day 2, the cells begin to proliferate on the printed surface, while the fibrin hydrogel is slowly biodegraded. IRS and SEM results show the biodegradation of fibrin is a sequence of events starting with the loss of water, leading to the shrinkage of the fibrin fibers, which in turn facilitates extensive intermolecular interactions and protein misfolding, yielding aggregated β-sheet structures. The height of the drop changes after printing. Several factors influence these changes: cell migration and aggregation, stretching of the elastic fibrin fibers, the biodegradation process of the hydrogel, and cell proliferation. Because our samples were stored in supplemented DMEM in an incubator, the droplets did not dry. The sequence of morphological and structural changes in fibrin enables intercellular communication, forming an elastic 3D structure in which a growing number of cells accumulate. This fibrin structure dissolves slowly, creating space for the formation of cellular 3D networks. These structural fibrin changes may also affect cellular behavior. Our future long-term studies (over several days and weeks) will show how cell viability and, morphology, including extensions and cell-cell contacts, behave. Additionally, molecular changes in the cells will be analyzed using OMIC techniques. The goal is to ultimately generate a human 3D tissue model, for example, for the development of personalized pharmacological treatment strategies.

Summarizing, pneumatic conveying printing is a new inkjet drop-on-demand technique that operates on the mechanism of a drop ejection in a stream of gas, which proved to have a superb printing performance that is expressed by gentle cell-printing conditions (low velocity of the bioink drop in the gas stream, negligible shear stress and no exposure of the bioink to high pressure), applicability to viscous liquids (bioinks with a biological cell loads) and low cell-death rate during the printing process. It is well suited to the fabrication of models of tissues (e.g., skin) or cell aggregates. The technique has potential to print 3D features by layer by layer deposition of the hydrogel material. In initial tests two types of patterns, straight lines (distance of 4 mm between each other) and grids (5 × 5 mm) were printed from an acellular containing sodium alginate bioink. After the printing of each hydrogel layer, the surface was lightly misted with a solution of $CaCl_2$ to stabilize the freshly made alginate layer by cross-linking. The printed process was repeated up to 10 times, making structures of ca. 2-3 mm high in Z-direction.

Acknowledgments

We thank Jennifer Sevecke-Rave and Beate Bous for their excellent technical assistance. The authors acknowledge the Fluorescence Microscopy Service Unit, Carl von Ossietzky University of Oldenburg, for the use of the imaging facilities, specifically the FV3000. This system was funded by the DFG, the project number is 437530384. Special thanks to Dr. Levent Gütay from the Fluorescence Microscopy Core Facility for his extensive discussions about the best sample preparation and microscopy. The authors acknowledge the Electron and Light Microscopy Service Unit of the School of Mathematics and Science of the Carl von Ossietzky University for the use of the imaging facilities. We thank Eng. A. Brand for the discussions, design, and fabrication of a prototype of the new printing head. English-language services were provided by STELS-OL (desmosa@gmx.de).

Conflict of Interest

The authors do not have any conflict of interest including financial, personal or other relationships with other people or organizations.

Ethics Statement

No human material was used in this study.

References

[1] Barrs R W, Jia J, Silver S E, Yost M and Mei Y 2020 *Chem. Rev.* **120** 10887-949
[2] Li X, Liu B, Pei B, Chen J, Zhou D, Peng J, Zhang X, Jia W and Xu T 2020 *Chem. Rev.* **120** 10793-833
[3] Mota C, Camarero-Espinosa S, Baker M B, Wieringa P and Moroni L 2020 *Chem. Rev.* **120** 10547−607
[4] Sun W, Starly B, Daly A C, Burdick J A, Groll J, Skeldon G, Shu W, Sakai Y, Shinohara M, Nishikawa M, Jang J, Cho D W, Nie M, Takeuchi S, Ostrovidov S, Khademhosseini A, Kamm R D, Mironov V, Moroni L and Ozbolat I T 2020 *Biofabrication* **12** 022002/1-33
[5] Ribeiro A, Blokzijl M M, Levato R, Visser C W, Castilho M, Hennink W E, Vermonden T and Malda J 2018 *Biofabrication* **10** 014102
[6] Kumar P, Ebbens S and Zhao X 2021 *Bioprinting* **23** e00157
[7] DeMel D C, Wagner G A, Maresca J A and Geibel J P 2023 *BioTechniques* **76** 53-62
[8] Lee J M, Huang X, Goh G L, Tran T and Yeong W Y 2023 *Int. J. Bioprinting* **9** 758
[9] Prabhakaran P, Palaniyandi T, Kanagavalli B, Ram kumar V, Hari R, Sandhiya V, Baskar G, Kumar Rajendran B and Sivaji A 2022 *Acta Histochemica* **124** 151932
[10] Takagi D, Lin W, Matsumoto T, Yaginuma H, Hemmi N, Hatada S and Seo M 2019 *Int. J. Bioprinting* **5** 208
[11] Blaeser A, Duarte Campos D F, Puster U, Richtering W, Stevens M W and Fischer H 2016 *Adv. Healthc. Mater.* **5** 326–33
[12] Negro A, Cherbuin T and Lutolf M P 2018 *Sci. Rep.* **8** 17099
[13] https://www.optica.org/History/Biographies/bios/Ichiro_Endo 2023 Optica, History, Biographies, Ichiro Endo.
[14] https://www.optica.org/history/biographies/bios/john_vaught/ 2023 Optica, History, Biography, John Vaught.
[15] Hutchings I M and Martin G D 2012 *Inkjet technology for digital fabrication*: Wiley)
[16] Ji S and Guvendiren M 2017 *Front. Bioeng. Biotechnol.* **5** Artcile 23
[17] Tong A, Pham Q L, Abatemarco P, Mathew A, Gupta D, Iyer S and Voronov R 2021 *SLAS Technology* **26** 333--66
[18] Xu C, Zhang M, Huang Y, Ogale A, Fu J and Markwald R R 2014 *Langmuir* **30** 9130−8
[19] Shi J, Wu B, Li S, Song J, Song B and Lu W F 2018 *Biomed. Phys. Eng. Express* **4** 045028
[20] Faulkner-Jones A, Courtney A, Cornelissen D J, Gardner J, King J, Fyfe C and Shu W 2015 *Biofabrication* **7** 044102
[21] Mancha Sánchez E, Gómez-Blanco J C, López Nieto E, Casado J G, Macias-Garcia A, Diaz Diez M A, Carrasco-Amador J P, Torrejon Martin D, Sánchez-Margallo F M and Pagador J B 2020 *Front. Bioeng. Biotechnol.* **8** 776
[22] Xie M, Su J, Zhou S, Li J and Zhang K 2023 *Gels* **9** 88
[23] Adamson A W and Gast A P 1997 *Physical Chemistry of Surfaces*: Wiley)
[24] Jungst T, Smolan W, Schacht K, Scheibel T and Groll J 2016 *Chem. Rev.* **116** 1496-539
[25] Rowley J A, Madlambayan G and Mooney D J 1999 *Biomaterials* **20** 45-53
[26] Emami Z, Ehsani M, Zandi M and Foudazi R 2018 *Carbohydr. Polym.* **198** 509-17
[27] Zhao H, Ma L, Zhou J, Mao Z, Gao C and Shen J 2008 *Biomed. Mater.* **3** 015001/1-9
[28] Sproul E, Nandi S and Brown A 2018 *Peptides and Proteins as Biomaterials for Tissue Regeneration and Repair*, ed M A Barbosa and M C L Martins (Duxford: Elsevier) pp 151-73
[29] Weisel J W 2004 *Biophys.Chem.* **112** 267-76
[30] Weisel J W and Litvinov R I 2017 *Subcell Biochemistry* **82** 405–56
[31] de Melo B A G, Jodat Y a, Cruz E M, Benincasa J C, Shin S R and Porcionatto M A 2020 *Acta Biomaterialia* **117** 60-76
[32] Brown A E X, Litvinov R I, Discher D E, Purohit P K and Weisel J W 2009 *Science* **325** 741-4
[33] Zhmurov A, Kononova O, Litvinov R I, Dima R I, Barsegov V and Weisel J W 2012 *J. Am. Chem. Soc.* **134** 20396−402
[34] Liu Y F, Pai Y F, Tsai M H and Hwang W S 2012 *Appl. Phys. A* **109** 323–9
[35] Park J A, Yoon S, Kwon J, Now H, Kim J K, Kim W J, Yoo J Y and Jung S 2017 *Sci. Rep.* **7** 14610/1-11
[36] Christensen K, Compaan A, Chai W, Xia G and Huang Y 2017 *ACS Biomater. Sci. Eng* **3** 3687−94
[37] Yoon S, Park J A, Lee H R, Yoon W H, Hwang D S and Jung S 2018 *Adv. Healthc. Mater.* **7** 1800050/1-10
[38] Brand I, Groß I, Li D, Zhang Y and Bräuer A U 2019 *RSC Adv.* **9** 40910-6
[39] Zhang Y, Li D, Liu Y and Wittstock G 2018 *Small* **14** 1802583/1-7
[40] De Maria C, Ferrari L, Montemurro F, Vozzi F, Guerrazzi I, Boland T and Vozzi G 2015 *Procedia Eng.* **110** 98-105
[41] Yamaguchi S, Ueno A, Akiyama Y and Morishima K 2012 *Biofabrication* **4** 045005
[42] Malda J, Visser J, Melchels F P, Jüngst T, Hennink W E, Dhert W J A, Groll J and Hutmacher D W 2013 *Adv. Mater.* **25** 5011-28

[43] Ferris C J, Gilmore K J, Beirne S, McCallum D, Wallace G G and Panhuis M i h 2013 *Biomaterials Science* **1** 224-30
[44] Jungst T, Smolan W, Schacht K, Scheibel T and Groll J 2016 *Chem. Rev.* **116** 1496-539
[45] Li D, Cao Y, Dong H, Wu X, Sun Q, Ma C, Huang B, Rastgar S, Wittstock G, Liu Y and Zhang Y 2020 *Adv. Mater. Interfaces* **7** 1902131
[46] Jayasinghe S N, Qureshi A N and Eagles P A M 2006 *Small* **2** 216 – 9
[47] Xu C, Chai W, Huang Y and Markwald R R 2012 *Biotechnol. Bioeng.* **199** 3152-60
[48] Schindelin J, Arganda-Carreras I, Frise E, Kaynig V, Longair M, Pietzsch T, Preibisch S, Rueden C, Saalfeld S, Schmid B, Tinevez J Y, White D J, Hartenstein V, Eliceiri K, Tomancak P and Cardona A 2012 *Nature Methods* **9** 676–82
[49] Wang Q, Liao Y, Jin W, Ho Y, Wang K, Guan Y and Fu W 2023 *Phys. Fluids* **35** 082007
[50] Gao G, Yonezawa T, Hubbell C, Dai.G. and Cui X 2015 *Biotechnol. J.* **10** 1568-77
[51] Cui X, Dean D, Ruggeri Z M and Boland T 2010 *Biotechnol. Bioeng.* **106** 963-9
[52] van Oss C J 1990 *J. Protein Chem.* **9** 487-91
[53] Amirfazli A and Neumann A W 2004 *Adv. Colloid Interface Sci.* **110** 121–41
[54] Drelich J 1996 *Colloids Surf., A* **116** 43-54
[55] Marmur A 1997 *J. Colloid Interface. Sci*, **186** 462–6
[56] https://www.thermofisher.com/content/dam/LifeTech/migration/en/filelibrary/cell-tissue-analysis/pdfs.par.85861.file.dat/hek-293.pdf
[57] www.cytion.com 2024 Cytion.
[58] Clapham D E 2007 *Cell* **131** 1047-58
[59] Goodenough D A and Paul D L 2003 *Nat. Rev.* **4** 1-10
[60] Humeau J, Bravo-San Pedro J M, Vitale I, Nunez L, Villalobos C and Senovilla L 2018 *Cell Calcium* **70** 3-15
[61] Orrenius S, Zhivotovsky B and Nicotera P 2003 *Nat. Rev.* **4** 552-65
[62] Posma J J N, Posthuma J J and Spronk H M H 2016 *J. Thromb. Haemost* **14** 1908-16
[63] Nierodzik M L and Karpatkin S 2006 *Cancer Cell* 355-62
[64] Laposata M, Dovnarsky D K and Shin H S 1983 *Blood* **62** 549-56
[65] Liu J, Schuff-Werner P and Steiner M 2006 *Biochem. Biophys. Res. Commun.* **343** 183–9
[66] McNamara C A, Sarembock I J, Gimple L W, Fento 2nd J W, Coughlin S R and Owensil G K 1993 *J. Clin. Invest.* **91** 94-8
[67] Piechocka I K, Bacabac R G, Potters M, MacKintosh F C and Koenderink G H 2010 *Biophys. J.* **98** 2281-9
[68] Baradet T C, Haselgrove J C and Weisel J W 1995 *Biophys. J.* **68** 1551-60
[69] Collet J P, Park D, Lesty C, Soria J, Soria C, Montalescot G and Weisel J W 2000 *Atertio. Thromb. Vasc. Biol.* **20** 1354-61
[70] Collet J P, Shuman H, Ledger R E, Lee S and Weisel J W 2005 *Proc. Natl. Acad. Sci.* **102** 9133-7
[71] Daraei A, Pieters M, Baker S R, de Lange-Loots Z, 2, Aleksander Siniarski 5,6 and Rustem I. Litvinov 7 C S B V, Moniek P. M. de Maat 8 , John W. Weisel 7, Robert A. S. Ariëns 4 and Martin Guthold 1 *Biomolecules*
[72] Domingues M M, Macrae F L, Duval C, McPherson H R, Bridge K I, Ajjan R A, Ridger V C, Connell S D, Philippou H and Ariens R A S 2016 *Thrombosis and Haemostasis* **127** 487-95
[73] Bannish B E, Paynter B, Risman R A, Shroff M and Tutwiler V 2024 *Biophys. J.* **123** 610–21
[74] Bauer R, Hansen S L, Jones G, Suenson E, Thorsen S and Ogendal L 1994 *Eur. Biophys. J.* **23** 239-52
[75] Barth A and Zscherp C 2002 *Q. Rev. Biophys.* **35** 369-430
[76] Tatulian S A 2013 *Lipid-protein interactions. Methods and protocols,* ed J H Kleinschmidt (New York: Springer) pp 177-218
[77] Bramanti E, Benedetti E, Sagripanti A, Papineschi F and Benedetti E 1997 *Biopolymers* **41** 545-53
[78] Desroches M J, Chaudhary N and Omanovic S 2007 *Biomacromolecules* **8** 2836-44
[79] Bagchi S, Falvo C, Mukamel S and Hochstrasser R M 2009 *J. Phys.Chem. B* **113** 11260–73
[80] Yu C C, Chiang K Y, Okuno M, Seki T, Ohto T, Yu X, Korepanov V, Hamaguchi H, Bonn M, Hunger J and Nagata Y 2020 *Nat. Commun.* **11** 5977/1-8
[81] Seki T, Chiang K Y, Yu C C, Yu X, Okuno M, Hunger J, Nagata Y and Bonn M 2020 *J. Phys.Chem. Lett.* **11** 8459–69
[82] Tong Y Y J, Kampfrath T and Campen K 2016 *Phys Chem Chem Phys* **18** 18424-30
[83] Detsch R, Blob S, Zehnder T and Baoccaccini A R 2016 *BioNanoMat* **17** 185-91
[84] Cui X, Breitenkamp K, Finn M G, Lotz M and D'Lima D D 2012 *Tissue Eng. A* **18** 1304-12
[85] Ablanedo Morales P, Rodriguez B, Furth M E, Molina K B, Boland A J, Mohl J E and Boland T 2023 *Biofabrication* **15** 031001
[86] Jayasinghe S N 2007 *Biotechnol. J.* **2** 934–7
[87] Chaudhary G, Luo R, George M, Tescione L, Khetan A and Lin H 2020 *Biotechnol. Bioeng.* **117** 1684–95
[88] Zhu Y, Cuenca J V, Zhou W and Varma A 2008 *Biotechnol. Bioeng.* **101** 751-69

[89] Tirella A, Vozzi F, De Maria C, Vozzi G, Sandri T, Sassano D, Cognolato L and Ahluwalia A 2011 *Journal of Bioscience and Bioengineering* **112** 79-85
[90] Zhang Y, O'Mahony A, He Y and Barber T 2024 *Biofabrication* **16** 022003
[91] Parsa S, Gupta M, Loizeau F and Cheung K C 2010 *Biofabrication* **2** 025003/1-8
[92] Xu H, Liu J, Shahriar M and Xu C 2023 *Langmuir* **39** 545-55